Stem cell therapy for cardiovascular disease : answering basic questions regarding cell behavior

Bogt, K.E.A. van der

CHAPTER 8

Micro Computed Tomography for Characterization of Murine Cardiovascular Disease Models

Ahmad Y. Sheikh*, Koen E.A. van der Bogt*, Timothy C. Doyle,
Maryam K. Sheikh, Katherine J. Ransohoff, Ziad A. Ali, Owen P. Palmer,
Robert C. Robbins, Michael P. Fischbein and Joseph C. Wu

Journal of the American College of Cardiology:
Cardiovascular Imaging 2010 Jul;3(7):783-5

*Both authors contributed equally to this study

LETTER TO THE EDITOR

It can hardly be argued that cardiac imaging methodologies targeting small animal models have been crucial for rapidly transitioning therapies from the bench to bedside. The adaptation of ultrasound for imaging murine hearts, for example, has allowed characterization of the developing and adult rodent heart, making it an essential tool for the study of developmental biology and cardiovascular disease. Nevertheless, additional imaging tools may prove useful adjuncts and/or alternatives to such established traditional modalities.

Ideally, a cardiovascular imaging modality should provide structural-functional quantitation, and be non-invasive, fast, cost-effective, precise, and accurate. While the combination of echocardiography and small animal cardiac MRI has proven to meet several of these criteria, there is certainly room for other modalities to be employed as well. At our institution, experimentation with a Micro-CT scanner eventually produced contrast-enhanced, high-resolution 3-dimensional imaging of the murine heart and associated structures. Indeed, early success with CT imaging of murine hearts has also been described in limited detail by other investigators [1,2] but to our knowledge, a validation of this technique by direct comparison to multiple established methodologies has not been described. Hence, we present the first study aimed to directly compare this novel imaging modality with both conventional echocardiography and conductance catheter (CC) measurement techniques using an established murine model of ischemic heart disease. Specifically, we have tested the hypothesis that Micro-CT can provide reliable information about ventricular structure and function following surgical LAD-ligation induced myocardial infarction (MI) in mice.

We randomized adult (8-10 weeks old) female FVB mice (n=19) to surgical LAD ligation or sham procedure. Dual cardiac and respiratory gated, IV contrast enhanced (20 µL/g Fenestra VC; ART Inc., Montreal, Canada) CT scans were performed pre-operatively and at 4, 8, and 12 weeks post-procedure using the eXplore Locus RS150 MicroCT (GE Healthcare, Fairfield, CT). Scans were performed with a 70 kVp, 40 mAmp x-ray source, acquiring 286 views over 200°, averaging two frames per view, 4x4 binning on the CCD detector. The heart was centered in a 46.25 mm axial field of view (84.7 mm trans-axial FOV), and sub-regions of the scanned data were reconstructed at an isotropic resolution of 97.3 µm. End-diastolic and end-systolic images were prospectively acquired with a temporal resolution of 15 milliseconds (ms) by gating on ECG P- and S'-waves, respectively (see **figure 1a-b** for animal set-up and gating reference). Continual imaging of the cardiac cycle (at 10-15 ms intervals) was also conducted of a representative animal at each time point (**figure 2** demonstrates continuous imaging of control animal). Post-acquisition analysis was performed using GE image analysis software (**figure 1c-d**).

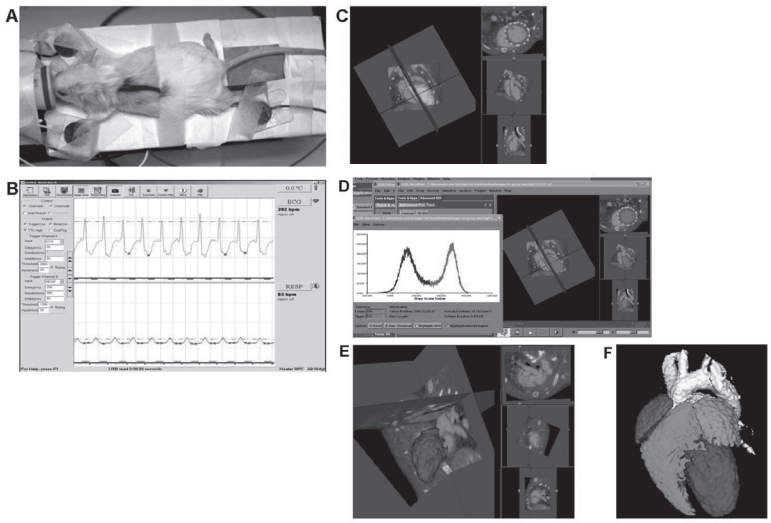

Figure 1. Outline of image acquisition and processing by Micro-CT. (a) Mouse positioned on CT scanner bed with 3 lead ECG. (b) Screen shot of ECG (top) and respiratory (bottom) tracings. Red squares occurring at the same time in both ECG and respiratory tracings indicate image acquisition points during maximum LV contraction (S') and inspiration. (c) Region of interest (orange dots) created around heart chamber (LV shown). (d) Histogram used to isolate voxels representing chamber volume. (e) Rendered surface of blood within chamber (LV). (f) Representative composite image of cardiac chambers and great vessels.

All operators obtaining and analyzing the CT scans were able to obtain measurements with minimal variability (±0.5-4.0%, data not shown). Echocardiography was performed by obtaining three independent two-dimensional transversal-targeted M-mode traces at the level of the papillary muscles using a 14.7-MHz transducer on a Sequoia C512 Echocardiography system (Siemens, Malvern, PA, USA). Using the Siemens proprietary software, left ventricular end-diastolic and end-systolic posterior and anterior dimensions were measured and processed to calculate left ventricular fractional shortening (LVFS). Invasive, steady-state hemodynamic measurements were conducted by closed-chest pressure-volume (PV) loop analysis using a 1.4-F conductance catheter (Millar Instruments, Houston, TX, USA) at week 12. These data were analyzed using PVAN 3.4 Software (Millar Instruments, Houston, TX, USA) and Chart/Scope Software (AD Instruments, Colorado Springs, CO, USA).

Mean left ventricular diastolic (LVDV) and systolic (LVSV) volumes were not significantly different between the sham and MI groups at baseline (37.2±2.0 µL vs. 39.7±1.8 µL in diastole and 11.2±0.6 µL vs. 11.4±0.8 µL in systole, respectively, *P*=NS). However, these volumes gradually increased in the MI group, finally reaching a mean diastolic value of 133.2±21.2 µL, compared to 55.4±1.0 µL in the sham operated group at 12 weeks post-operation (*P*=0.002, **figure 3a-c)**. Similarly, LVSV increased to 100.1±19.6 µL as compared to 19.9±1.2 µL in the sham group (*P*=0.002, **figure 3d**). This MI-induced increase in volumes mirrored functional failure, with deteriorating LVEF from an initial 70.6±2.5% to 26.2±2.8% after 12 weeks. By contrast, LVEF in the sham group remained around baseline (68.6±2.6%, *P*<0.0005, **Figure 3e**).

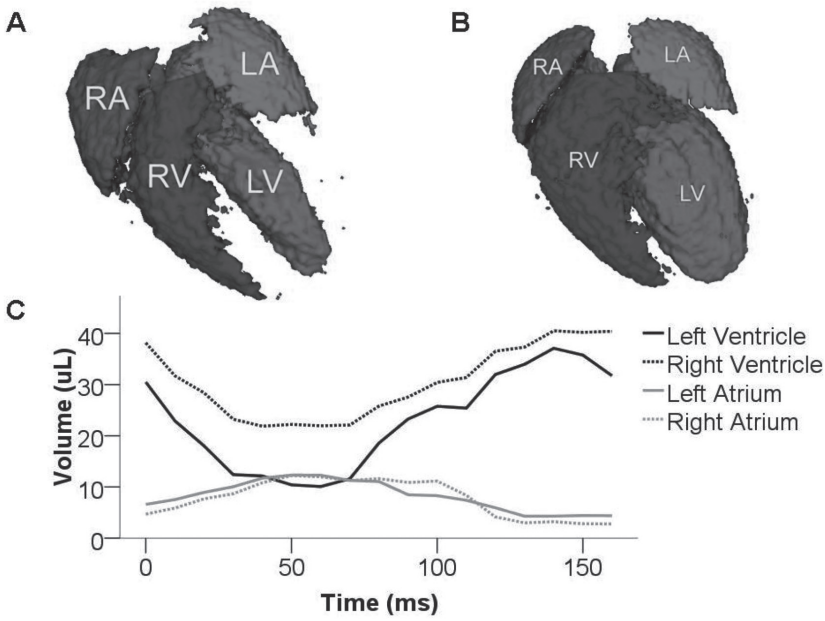

Figure 2. Quantification of cardiac chamber volumes by Micro-CT. Representative reconstruction of cardiac chamber volumes in (a) end-systole and (b) end-diastole allowed for extrapolation of chamber volumes and loading conditions during (c) the entire cardiac cycle.

As shown in **figure 4**, volumes measured by Micro-CT correlated well with dimensions acquired from echocardiography in both diastole (r^2=0.73) and systole (r^2=0.82). Similarly, volumes derived from the conductance catheter (CC)-based approach showed a correlative trend with those from the Micro-CT (r^2=0.83 in systole and r^2=0.81 in diastole). When volumes and dimensions were processed to calculate functional measurements of ventricular contraction, Micro-CT proved to correlate well with echocardiography (r^2=0.72, **figures 4d)**. These observations suggest that Micro-CT imaging can provide reliable volumetric assessment of cardiac chambers and ventricular function. For detailed echocardiography, CC, histological results, and representative images, please refer to **figures 5-7**.

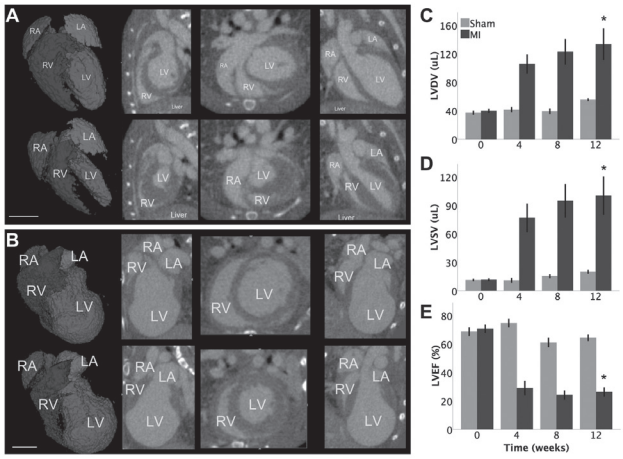

Figure 3: Gated Micro-CT provides insight into myocardial infarction-induced cardiac remodeling. (a) End diastolic (top row) and end systolic (bottom row) images of a normal mouse heart with chambers labeled in yellow. From left to right: rendered surface of blood volume, sagittal, axial, and coronal views. (b) Similar series of images from the same animal 12 weeks following LAD ligation (scale bar=5mm in both panels), showing clear signs of negative remodeling. (c) Graphic representation of increasing left ventricular diastolic volume (LVDV) over time following myocardial infarction as compared to relatively stable volumes in the sham-operated group. (d) Similarly, left ventricular systolic volume (LVSV) increased due to loss of cardiac muscle after infarction. (e) Myocardial infarction led to dilated cardiomyopathy with a significant loss of left ventricular ejection fraction (LVEF) as early as one month following LAD ligation (Bars represent mean±SE. *P<0.05 compared to sham group by repeated measurements ANOVA).

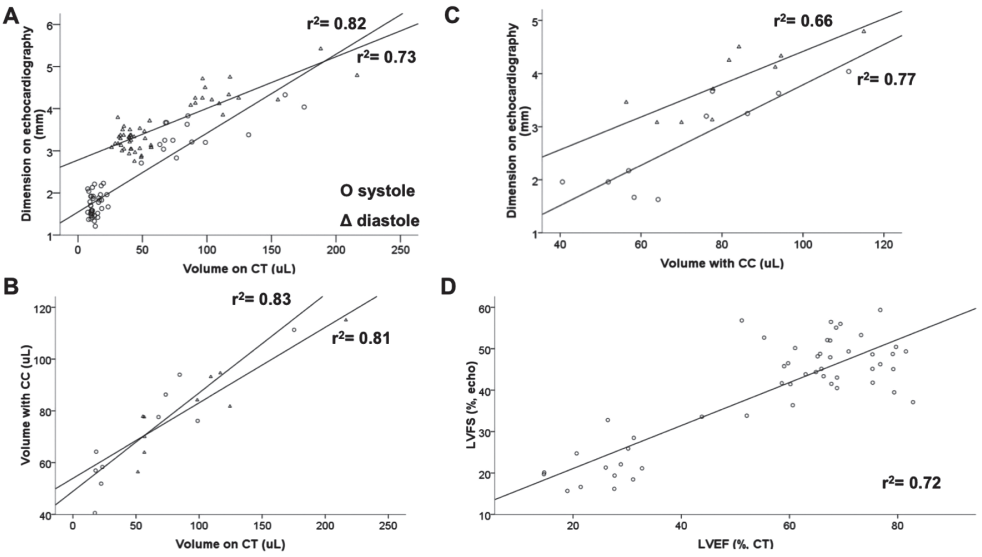

Figure 4. Micro-CT findings correlate robustly with established methods of measuring murine cardiac function. (a,b) Volumes derived from Micro-CT image analysis correlate well with dimensions measured using echocardiography and volumes assessed with the conductance catheter (CC) in both systole and diastole. (c) Echocardiography measurements of chamber length correlated well with volumes derived from CC measurements. (d) *In vivo* functional measurements from Micro-CT and echocardiography correlated well with a r^2 value of 0.72.

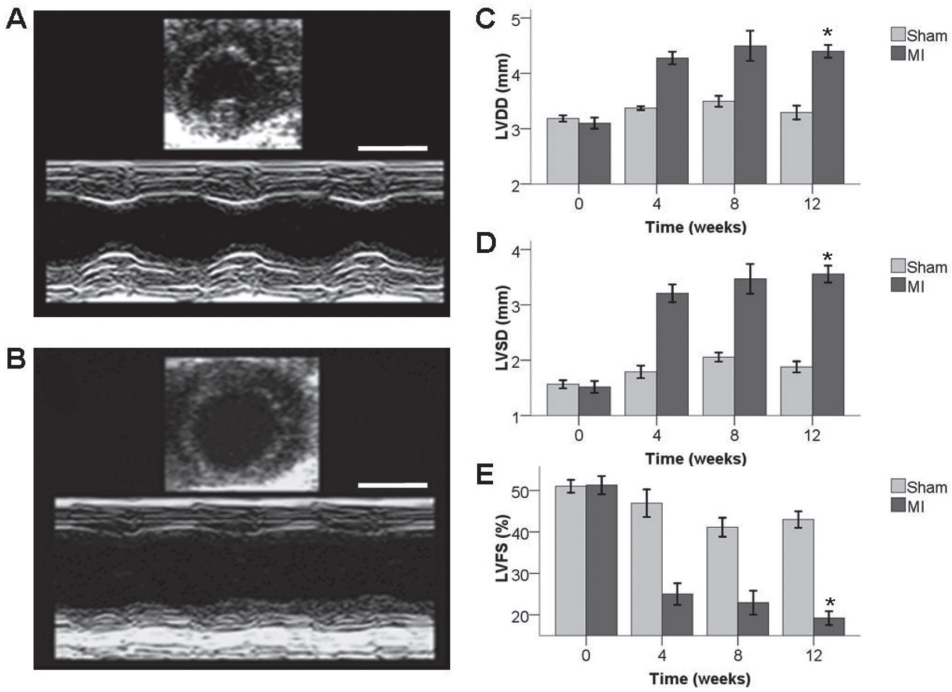

Figure 5. Echocardiographic M-mode traced measurements of ventricular diameters and calculated left ventricular fractional shortening (LVFS). (a) Representative M-mode traced picture taken at the level of the papillary muscle of a pre-operative heart whereby left ventricular diameters can be measured. Scale bar represents 5 mm. (b) The same heart as in (a) shows extensive dilatation at 12 weeks post-MI. (c-e) A gradual MI-induced increase in ventricular diameters in diastole (LVDD, c), and systole (LVSD, d) translated in a significantly compromised LVFS over a period of 12 weeks as compared to the sham group (Bars represent mean±SE. * represents $P<0.05$ compared to sham group by repeated measurements ANOVA).

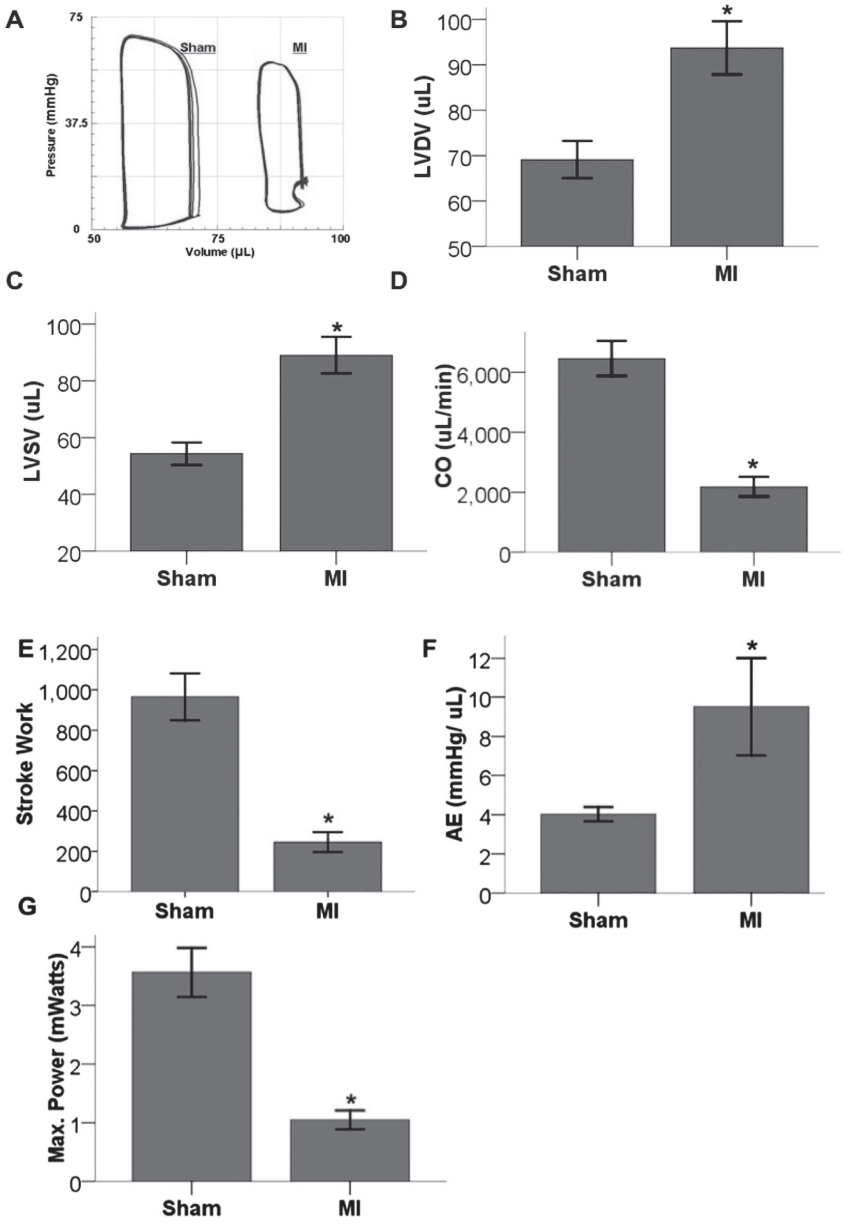

Figure 6. Conductance catheter (CC) based assessment of cardiovascular function. (a) Representative pressure-volume loops of sham (left) and MI (right) animals at 12 weeks post-MI, showing typical right shift indicating increased ventricular dilatation and volumes compared to pre-operative assessment. (b,c) Confirming findings by Micro-CT and echocardiography, extrapolation of pressure-volume loops showed significantly increased ventricular volumes in end-diastole (LVDV, B) and end-systole (LVSV, C) post-MI. (d,e) Cardiac output (CO)

as well as stroke work (SW) were both significantly diminished as well. (f) As a confirmatory measure of CHF, the arterial elastance (AE) was also significantly increased at the 12-week post-MI time point. (g) Finally, significantly decompensated MI-induced heart failure was illustrated by a markedly decreased maximum power generated by the left ventricle (Bars represent mean±SE. * represents P<0.05 compared to sham group by Student's t-test).

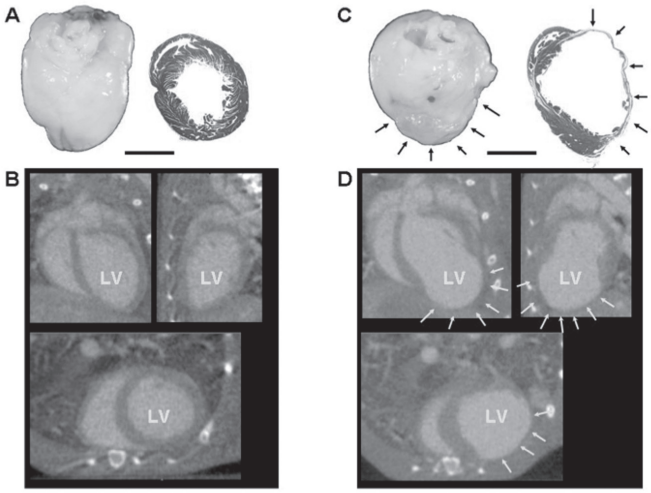

Figure 7. Post-mortem histological analysis confirms *in vivo* Micro-CT images. (a,b) Representative heart 12 weeks following sham procedure appears both grossly and histologically normal, corresponding to the *in vivo* images acquired by Micro-CT immediately prior to CC-measurements and sacrifice. (c) By contrast, a representative fixed heart 12 weeks post-infarction shows an aneurysmal, infarcted region and fibrosis on Masson-Trichrome staining (black arrows). (d) Corresponding *in vivo* Micro-CT images from the same heart with the infarcted area marked by yellow arrows clearly resembles the post-mortem images from (c). Scale bars represent 5 mm.

Over the past decade, cardiac CT has become an important clinical imaging modality for the characterization of cardiac structure and function, as well as coronary artery pathology [3, 4]. However, cardiac CT imaging has long been inapplicable to pre-clinical, small animal models due to the high spatial and temporal resolution required to visualize mouse hearts with rates of over 400 beats a minute. Recent advances in technology have allowed adaptation of CT imaging to the small animal laboratory, adding a valuable asset to the pre-clinical research tool chest. As shown in the present study, Micro-CT can provide accurate and precise measurements of the murine heart, and can serve as a useful adjunct to established measurements of cardiac function. Further refinements of this emerging technology are ongoing, and we predict that Micro-CT scanning will continue to be used in the small animal laboratory with increasing frequency.

REFERENCES:

1. Nahrendorf M, Badea C, Hedlund LW, Figueiredo JL, Sosnovik DE, Johnson GA, Weissleder R. High-resolution imaging of murine myocardial infarction with delayed-enhancement cine micro-CT. *Am J Physiol Heart Circ Physiol.* 2007;292(6):H3172-3178.
2. Detombe SA, Ford NL, Xiang F, Lu X, Feng Q, Drangova M. Longitudinal follow-up of cardiac structure and functional changes in an infarct mouse model using retrospectively gated micro-computed tomography. *Invest Radiol.* 2008;43(7):520-529.
3. Pouleur AC, le Polain de Waroux JB, Kefer J, Pasquet A, Vanoverschelde JL, Gerber BL. Direct comparison of whole-heart navigator-gated magnetic resonance coronary angiography and 40- and 64-slice multidetector row computed tomography to detect the coronary artery stenosis in patients scheduled for conventional coronary angiography. *Circ Cardiovasc Imaging.* 2008;1(2):114-121.
4. Ruzsics B, Lee H, Powers ER, Flohr TG, Costello P, Schoepf UJ. Images in cardiovascular medicine. Myocardial ischemia diagnosed by dual-energy computed tomography: correlation with single-photon emission computed tomography. *Circulation.* 2008;117(9):1244-1245.